

pubs.acs.org/NanoLett Letter

Photothermally Activated Artificial Neuromorphic Synapses

Brian W. Blankenship, Li, Ruihan Guo, Naichen Zhao, Jaeho Shin, Rundi Yang, Seung Hwan Ko, Junqiao Wu, Yoonsoo Rho, and Costas Grigoropoulos*



Cite This: https://doi.org/10.1021/acs.nanolett.3c02681



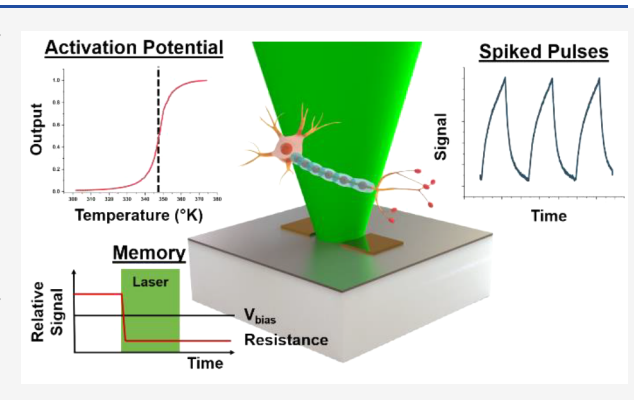
ACCESS I

III Metrics & More

Article Recommendations

s Supporting Information

ABSTRACT: Biological nervous systems rely on the coordination of billions of neurons with complex, dynamic connectivity to enable the ability to process information and form memories. In turn, artificial intelligence and neuromorphic computing platforms have sought to mimic biological cognition through software-based neural networks and hardware demonstrations utilizing memristive circuitry with fixed dynamics. To incorporate the advantages of tunable dynamic software implementations of neural networks into hardware, we develop a proof-of-concept artificial synapse with adaptable resistivity. This synapse leverages the photothermally induced local phase transition of VO₂ thin films by temporally modulated laser pulses. Such a process quickly modifies the conductivity of the film site-selectively by a factor of 500 to "activate" these neurons and store "memory" by applying



varying bias voltages to induce self-sustained Joule heating between electrodes after activation with a laser. These synapses are demonstrated to undergo a complete heating and cooling cycle in less than 120 ns.

KEYWORDS: neuromorphic devices, vanadium dioxide, artificial neural networks, photothermal electronics

Biological nervous systems are a marvel of complexity and efficiency, enabling organisms to perceive their environment, process sensory information, and make complex decisions in real time. Among its remarkable feats, the ability to process visual stimulus and rapidly generate appropriate responses stands out as a testament to the brain's incredible computational power. The visual system effortlessly handles an enormous volume of visual data, recognizing objects, detecting motion, and extracting meaningful patterns. 2-5

It has been a longstanding aspiration to replicate these sophisticated decision-making capabilities in artificial systems. Haded, the pursuit of replicating human thought processes has been a driving force behind the advancements in artificial intelligence. Software-based approaches have garnered incredible success in recent years in the fields of computer vision, natural language processing, and problem solving. However, the growing demand for lower latency and increasingly complex function has spurred interest in alternative approaches that emulate neuromorphic function at the hardware level. He fields of these, vanadium dioxide (VO₂) based memristors and oscillatory neural networks have attracted increasing interest.

VO₂ is a phase change material that experiences a rapid metal—insulator transition (MIT) that can be driven by external stimuli such as heat, ^{22,23} strain, ²⁴ and photo-excitation. ^{25,26} During this phase transition, VO₂ experiences a drastic change in both its electrical conductivity and optical absorptivity that is reversible upon the removal of a

stimulus.^{27–29} Conveniently, the MIT of VO₂ thin films occurs at relatively low temperatures ($T_c \approx 340 \text{ K}$). Typically, VO₂-based devices rely on Joule heating to modulate their resistivity for device functionality.³⁰

We present an approach utilizing both optical excitation and Joule heating to modulate the resistivity of a VO_2 electrode for fabricating an artificial synapse. This approach takes advantage of the unique and synergistic optical and electronic properties of VO_2 . Not only can the temperature changes required to fully modulate VO_2 across its MIT be accessed by relatively lowintensity laser excitation but also laser irradiation could potentially locally control the phase of VO_2 at ultrafast speeds. These benefits pave the way to create lower latency devices and sensors that have additional control parameters and with direct relevance for vision-related applications.

We identify and experimentally demonstrate three notable "neuromorphic" functionalities in our device. First, we suggest that VO₂ exhibits a nonlinear thresholding behavior that can produce adaptable and seemingly binarized outputs in a voltage divider circuit based on the application of sufficient

Received: July 18, 2023
Revised: September 9, 2023



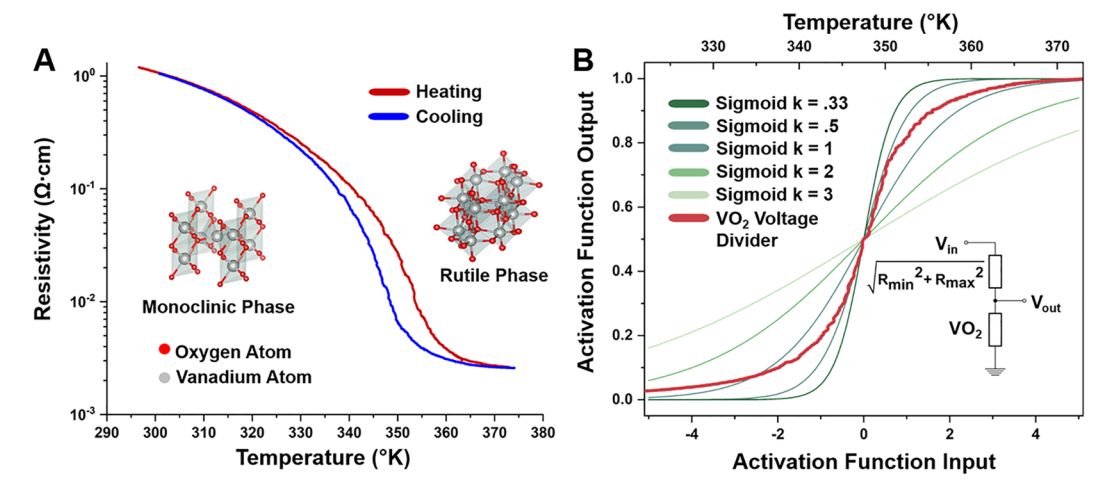


Figure 1. Nonlinear thresholding behavior. (A) Resistivity measurements of 150 nm thick VO_2 thin films on sapphire substrate. The resistivity of the VO_2 film changes by almost 3 orders of magnitude from ambient conditions (297 K) to 374 K as the film reorders from a monoclinic phase to a rutile phase. The resistivity exhibits a mild hysteresis in resistivity from heating to cooling. (B) By employing the VO_2 as a variable resistor in a simple voltage divider circuit we observe a sigmoidal response. We liken this response to sigmoidal activation functions commonly used for neural network and deep learning applications. The response of the VO_2 voltage divider circuit (red) is shown in comparison to sigmoid functions with steepness parameters between 0.33 and 3 (green).

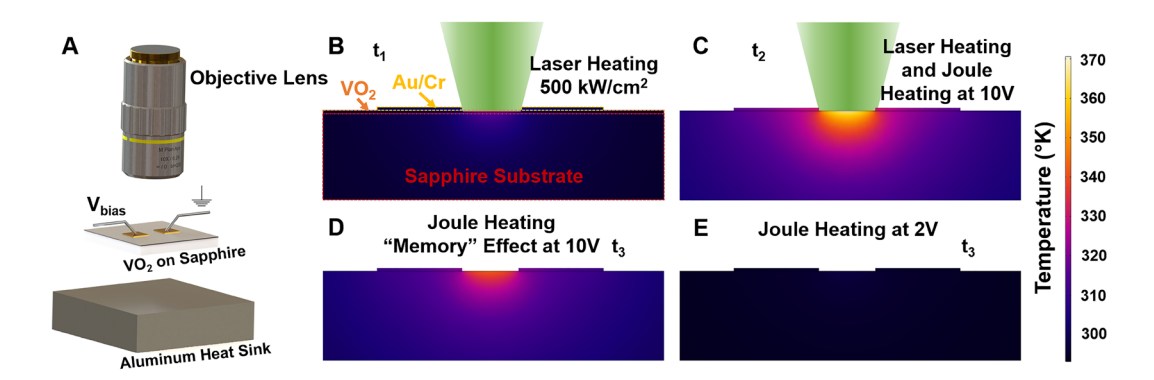


Figure 2. Memory effect simulations. (A) Model of electrodes on VO_2 film and heating elements. A laser can apply variable power to the VO_2 to generate heat on the surface while voltage can be applied across the electrodes to induce Joule heating. An aluminum heat sink is attached to better dissipate heat. (B) Without an applied bias voltage, a focused beam with intensity of 500 kW/cm² is only able to partially heat (\sim 323 K) the VO_2 film. (C) By applying a voltage across the electrodes, the partially heated film is conductive enough to induce substantial Joule heating that in turn raises the film temperature (370 K) until it reaches a steady-state temperature. (D) If the applied voltage is sufficient, the Joule heating in the conductive film is substantial enough for that to remain relatively conductive (E) whereas lower bias voltages are unable to sustain the necessary temperature to remain conductive and the VO_2 reverts to an insulating phase.

heat from a laser and subsequent Joule heating of the partially heated film between electrodes. Second, our observations indicate the presence of "memory" effects when varying biasing voltages are applied. These effects are manifested as the synaptic circuit remains in an "on" state even after the removal of the laser stimulus, highlighting the ability to retain information. Lastly, we show that these artificial synapses can react to thermal impulses in less than 120 ns for 10 μ m channels.

Our strategy for developing artificial synapses leverages the nonlinear resistivity of VO_2 as it undergoes its metal—insulator transition. During the phase transition, the lattice symmetry of VO_2 changes from a monoclinic phase to a rutile phase in a metallic state with an ~ 500 -fold change in resistivity. We utilize two complementary heating methods: selective laser heating of a VO_2 film positioned between two electrodes and Joule heating induced by the current flowing through the same electrodes. These heating mechanisms exhibit intricate

interdependence, whereby laser heating alters the temperature-dependent resistivity of VO_2 , resulting in an increased current flow, while the temperature dependence of the optical properties of VO_2 modifies its effective absorptivity. At time scales >10 ns that are explored in this paper, laser-induced phase transitions can be considered purely thermal in nature.

We first measure the resistivity of a 150 nm VO₂ thin film on a c-cut sapphire substrate. Information on the preparation of the thin film as well as the resistivity measurements are described in Materials and Methods). These measurements, shown in Figure 1A, agree with resistivity measurements found elsewhere in the literature for VO₂. Over the course of heating the film from 297 to 374 K the resistivity of the film decreases from 1.2 Ω cm to 2.58 \times 10⁻³ Ω cm with mild hysteresis as it is cooled back to ambient temperature.

By inserting this resistivity curve as a variable resistor element in a voltage divider with a normalized output, we observe an s-shaped response with respect to temperature.

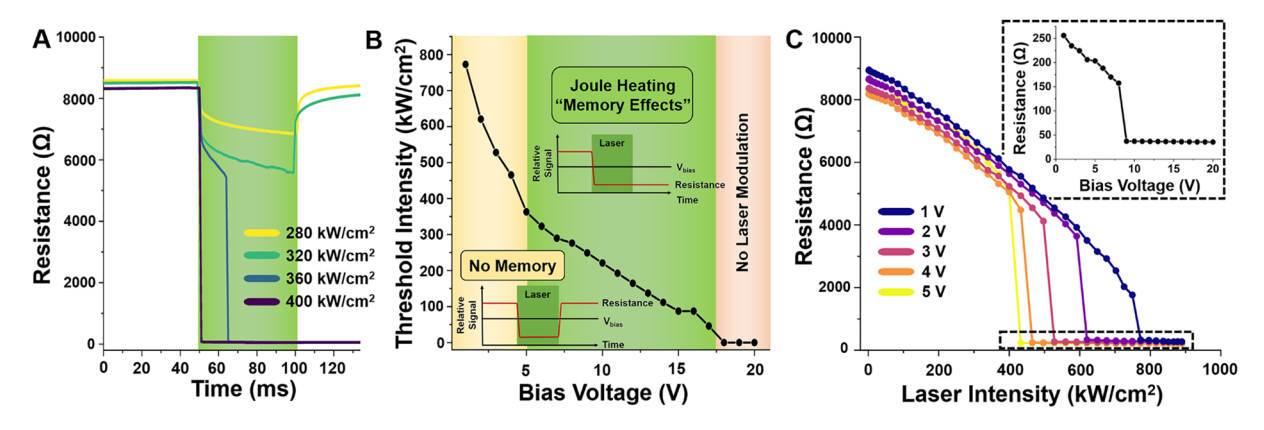


Figure 3. Memory effect. (A) Resistance between electrodes as a function of time by applying 50 ms pulses of 532 nm light of varying intensities. Above 360 kW/cm² the film is nearly instantaneously activated. (B) The thresholding laser intensity is explored for varying applied bias voltages. For bias voltages between 5 and 17 V (green region), a memory effect, described in Figure 3 is observed, and for bias voltages below 5 V there is still laser modulation of resistance based on the applied laser intensity (yellow region). However, above 17 V the synaptic circuit is activated without application of laser pulses (red region). (C) Resistance as a function of laser power and bias voltages measured from 1 to 5 V. The inset shows the steady-state resistance for different bias voltages measured at maximum applied laser intensity.

This analysis reveals that the response of this circuit exhibits remarkable similarity to sigmoid curves (see Figure 1B) of the form

$$f(x) = \frac{1}{1 + e^{-kx}} \tag{1}$$

and observe a best fit with a steepness parameter, k, of approximately 1.5. This result suggests that a thermally modulated VO_2 synaptic circuit can function as a hardware analogue to neural network activation functions. Thus, it is crucial to understand how to control the temperature within the film to effectively modulate its resistivity.

We pattern two 200 nm thick 15 μ m \times 15 μ m Cr/Au electrodes spaced 10 μ m apart onto the surface of the VO₂ (see Figure 2A) to apply a biasing voltage across electrodes and configure an artificial synapse that is activated by application of light between the electrodes. We can express the temperature across this synapse using a heat diffusion equation of the form

$$\rho C_{p}(T) \frac{\partial T}{\partial t} = \nabla \cdot (k(T)\nabla T) + Q_{abs}(x, y, z, T, t) + Q_{gen}(x, y, z, V, T, t)$$
(2)

where ρ , $C_{\rm p}$, K, and T represent density, specific heat, thermal conductivity, and temperature, respectively. $Q_{\rm abs}$ represents the volumetric energy intensity absorbed by the laser as a function of depth

$$Q_{abs}(x, y, z, T, t) = (\alpha(T)) \times I(x, y, t)e^{-\gamma |z|}$$
(3)

where α is the absorptivity as a function of temperature, I is the intensity of the impinging laser beam, and γ is the absorption coefficient. $Q_{\rm gen}$ in turn can be understood as the volumetric heat generation from Joule heating $\propto Vr(T)$ between electrodes as a function of the temperature in the synapse and applied bias voltage. Given that the resistivity and optical absorptivity are highly temperature dependent, these equations are nonlinear and can only be solved numerically.

To better understand temperature modulation dynamics across the synapse, we conduct time-dependent finite element analysis (details are given in the Supporting Information).

The results of these studies after 10 ms of simulated time are shown in Figure 2B-E. Upon laser heating with an intensity of 500 kW/cm² (Figure 2B) the VO₂ film is partially heated such that it becomes more conductive but does not fully undergo a transition into its conductive rutile phase. By applying a 10 V potential across the electrodes (Figure 2C), Joule heating substantially raises the temperature across the electrodes to the minimum observed resistivity from our measurements in Figure 1A. Interestingly, by then removing the laser (Figure 2D), the Joule heating in the heated, conductive film is able to reach a steady-state temperature beyond the MIT temperature and the synapse remains "on" as the temperature and resistivity of the film marginally decreases. We ascribe this to a "memory" effect. If the bias voltage is not sufficient (Figure 2E), Joule heating is not able to sustain a temperature for the film to remain conductive. We note that by itself, the Joule heating from bias voltages below ~17 V from an unheated film is unable to reach the MIT temperatures because the initial conductivity is low. This highlights the inherent nonlinear thresholding arising from the duality of laser and Joule heating.

Following these simulation results, we performed physical measurements on our device, to validate and further investigate its actual behavior. To understand the necessary laser intensities to activate the synaptic circuit, we first applied a 5 V DC bias across the electrodes and varied the applied intensity of laser pulses (Figure 3A). We observe that at lower laser intensities (<320 kW/cm²), the resistance across the electrodes plateaus across time to values within an order of magnitude of the original resistance. However, when applying a 360 kW/cm² pulse, we initially observe a similar plateauing at lower power intensities, followed by an abrupt change in resistance to ~200 Ω . Likewise, when applying higher intensity pulses (400 kW/cm²), the synapses reach resistances of around 200 Ω within 1 ms.

Figure 3B depicts the threshold laser intensities necessary to activate within 1 ms for different bias voltages (green region). There is a decreasing trend of threshold intensity for increasing bias voltage as Joule heating contributes more heat at higher bias voltages. In the low bias voltage regime (<5 V) laser heating can actively modulate the resistance between electrodes, but the Joule heating is unable to sustain the necessary temperature to produce the "memory" effects discussed

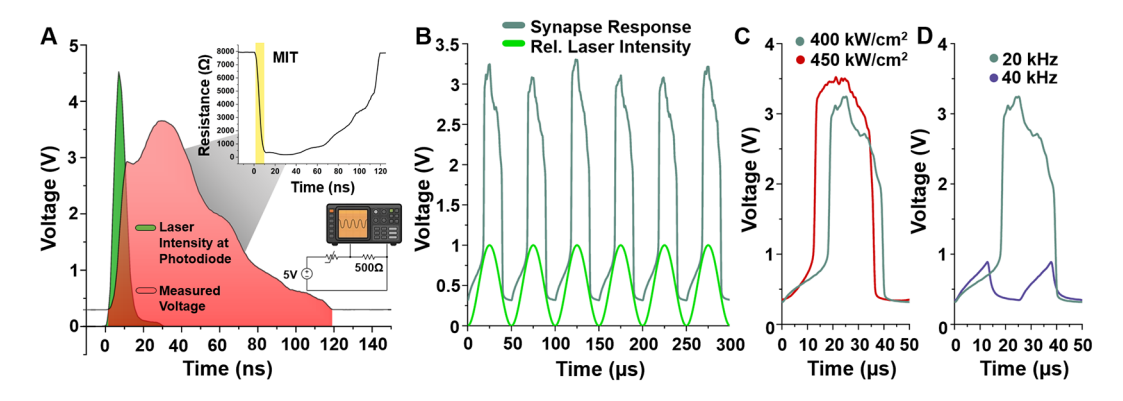


Figure 4. Spiking behavior. (A) Voltage response of the synaptic circuit (red) from excitation from a 7 ns laser pulse (green). Voltage output is converted into a corresponding resistance value shown in the top right. (B) Voltage "spikes" in the synaptic circuit from periodic microsecond laser excitation at 400 kW/cm² with a constant 5 V applied bias voltage (green). (C) By increasing the power of the laser pulse, the spike is seen to activate more quickly (red). (D) Comparison of voltage responses from a 20 kHz pulse and a 40 kHz pulse (purple). In the latter case, we see an incomplete metal—insulator transition within each pulse.

previously (yellow region). In the range of 5–17 V, the memory effects are observed, and beyond 17 V, the electrodes are activated without any stimulus from the laser pulse (red region). More precise measurements of the resistance as a function of laser power for different bias voltages are shown in Figure 3C. In this case, sharp drops in the resistance are observed between electrodes from only minor increases in applied laser intensity. The inset in Figure 3C highlights the steady-state resistance as a function of bias voltage, where a minimum resistance of ~37 Ω is measured at bias voltages >9 V.

To understand the thermal response behavior within a submicrosecond time regime, we first apply a 7 ns fwhm 532 nm pulse with $\sim 10 \text{ mJ/cm}^2$ fluence that was found to be slightly above the threshold fluence to activate the synapse. The time-dependent resistivity change from this pulse with 5 V bias is recorded in Figure 4A. These data elucidate the transient behavior of the synapse. The response is marked by rapid thermalization during the duration of the pulse, followed by the onset of Joule heating after approximately 16 ns from the start of the pulse. The synapse reaches its minimum resistivity after 30 ns and subsequently begins cooling back to ambient temperature as the Joule heating is unable to sustain itself. The cycle of heating and cooling to ambient takes a minimum of 120 ns, although we expect to be able to tailor this by using substrates with differing thermal conductivities and contact resistances.

Moreover, we employ an electro-optical modulator (EOM) to modulate a continuous wave (CW) beam, aiming to rapidly activate and reactivate the synaptic circuit. The utilization of the EOM allows precise manipulation of laser power at kilohertz pulse frequencies that we investigate. We aim to demonstrate the synapse's ability to generate "spikes" with tailorable rise times and shapes that could be used to encode information in neuromorphic computing models by controlling parameters in the synaptic circuit. Considering that spike encoding offers an efficient method for representing temporal information, it holds potential for real-time sensory processing, pattern recognition, and information transmission applications.

Using the same voltage divider circuit as displayed in Figure 4A, we first measure the voltage response from periodic 20 kHz laser excitation with base laser intensity of 400 kW/cm² (Figure 4B). The synapse is shown to reproduce consistently

shaped pulses across time. The extent of the heat-affected zone into the substrate is approximately proportional to $\sqrt{\alpha t}$, where α is the thermal diffusivity of the substrate. In this case, the heat-affected zone corresponding to the microsecond pulse is significantly larger than the corresponding heating from the nanosecond pulse, leading to longer microsecond-regime cooling times. Figure 4C compares the voltage response of a single spike from a base of 400 kW/cm² to a 450 kW/cm² pulse at the same frequency. These results show that the rise time of the pulse from the onset of laser heating can be shortened by applying higher intensity pulses. Figure 4D shows the effect of increasing the pulse frequency on the shape of the voltage spikes for a beam of the same base intensity. Beyond ~40 kHz pulse frequency, the spike loses its dynamic range and produces sawtooth-like responses as the VO₂ film no longer fully undergoes MIT. Likewise, these higher frequency pulses experience heat accumulation effects over time where the minimum resistivity across pulses is lower than for lower frequency pulses. The corresponding resistivity curves of these pulses are shown in Figure S4.

Our study presents an approach for developing an artificial neuromorphic synapse that offers a wide dynamic range of resistivities through the application of varying intensities of light and bias voltages. We have demonstrated three distinct "neuromorphic" functionalities of this circuit including binary thresholding, memory, and spike encoding. Moreover, we have characterized the circuit's electrical response to varying applied laser intensities, bias voltages, and pulse frequencies. Our results suggest that these synapses can be thermally activated by a laser in under 35 ns and retain memory at bias voltages as low as 5 V. We have shown that information can be effectively encoded as unique "spikes" possessing different shapes and attributes based on the duration and intensity of the applied laser pulse. There is still considerable room to design practical sensing and computing devices and explore the possibility of making rewireable circuits using spatially modulated light between sets of electrodes as well as making more favorable substrates and device geometries.

Materials and Methods. The 150 nm VO_2 thin films were grown on c-cut sapphire substrates using pulsed laser deposition (PLD) with a 248 nm KrF excimer laser. The laser energy was set to be 321 mJ with 10 Hz pulse frequency. Thin films were deposited in a 5 mTorr O_2 environment at 485

 $^{\circ}$ C for 20 min. Subsequently, a postdeposition annealing process was performed in the same 5 mTorr O_2 environment at 485 $^{\circ}$ C for 20 min.

AZ MIR701 photoresist was patterned onto a 1 cm \times 1 cm, 150 nm thick VO $_2$ thin film using standard single-layer photolithography processes shown in Figure S1. Afterward a 200 nm thick Cr/Au layer was deposited as an electrode. A variety of electrode geometries were patterned to determine optimal electrode spacing and path lengths. The chip was attached to a 2 mm thick piece of aluminum by silver thermal paste to act as a heat sink.

The temperature dependence of resistance on the VO_2 film was measured using a Miller FPP-5000 four-point measurement probe and controlling the temperature by a thin Peltier heater/cooler. The temperature was measured using a k-type thermocouple and cycled between room temperature and 375 K at a rate of 25 K/min with a PID controller.

The experimental setup is shown in Figure S2. A CW or nanosecond laser beam is first linearly polarized and travels through an EOM to change polarization. The output beam travels through a polarized beam splitter to modulate power. One arm of the beam serves to measure power, which is used to calibrate the power of the forward beam. The beam is ultimately focused onto a Mitutoyo 10× objective onto a chip carrier containing an array of synapses. The terminals of this chip carrier are then routed to either a Keithley 2401 source measurement for measurements with >1 ms measurement intervals unit or an oscilloscope for submillisecond resistance measurements.

ASSOCIATED CONTENT

Supporting Information

The Supporting Information is available free of charge at https://pubs.acs.org/doi/10.1021/acs.nanolett.3c02681.

Device patterning information, experimental setup diagrams, simulation information, resistivity curves from periodic laser heating, and a diagram illustrating a potential application for heating with spatially modulated light (PDF)

AUTHOR INFORMATION

Corresponding Authors

Costas Grigoropoulos — Laser Thermal Laboratory, Department of Mechanical Engineering, University of California, Berkeley, California 94720, United States; orcid.org/0000-0002-8505-4037; Email: cgrigoro@berkeley.edu

Yoonsoo Rho — Laser Thermal Laboratory, Department of Mechanical Engineering, University of California, Berkeley, California 94720, United States; Physical & Life Sciences and NIF & Photon Sciences, Lawrence Livermore National Laboratory, Livermore, California 94550, United States; Email: rho1@llnl.gov

Authors

Brian W. Blankenship — Laser Thermal Laboratory, Department of Mechanical Engineering, University of California, Berkeley, California 94720, United States; orcid.org/0000-0003-4212-6835

Runxuan Li – Laser Thermal Laboratory, Department of Mechanical Engineering, University of California, Berkeley, California 94720, United States

- Ruihan Guo Department of Materials Science and Engineering, University of California, Berkeley, California 94720, United States
- Naichen Zhao Laser Thermal Laboratory, Department of Mechanical Engineering, University of California, Berkeley, California 94720, United States
- Jaeho Shin Applied Nano and Thermal Science Lab, Department of Mechanical Engineering, Seoul National University, Seoul 08826, South Korea
- Rundi Yang Laser Thermal Laboratory, Department of Mechanical Engineering, University of California, Berkeley, California 94720, United States; orcid.org/0000-0002-2877-939X
- Seung Hwan Ko − Applied Nano and Thermal Science Lab, Department of Mechanical Engineering, Seoul National University, Seoul 08826, South Korea; orcid.org/0000-0002-7477-0820
- Junqiao Wu Department of Materials Science and Engineering, University of California, Berkeley, California 94720, United States; orcid.org/0000-0002-1498-0148

Complete contact information is available at: https://pubs.acs.org/10.1021/acs.nanolett.3c02681

Author Contributions

 $^{\perp}$ B.W.B. and R.L. contributed equally.

Notes

The authors declare no competing financial interest.

ACKNOWLEDGMENTS

B.W.B. acknowledges support from the US NSF Graduate Research Fellowship (DGE 2146752). We acknowledge support to the Laser Thermal Laboratory by the US NSF under grant CMMI-2024391. Device fabrication and $\rm VO_2$ synthesis was performed at UC Berkeley's Marvell Nanofabrication Laboratory and the Biomolecular Nanotechnology Center of the California Institute for Quantitative Biosciences. We also acknowledge the Molecular Graphics and Computation Facility under NIH S10OD034382 for COMSOL usage.

■ REFERENCES

- (1) Kandel, E. R.; Schwartz, J. H.; Jessell, T. M. Principles of neural science, 4th ed.; McGraw-Hill, Health Professions Division: 2000.
- (2) Barlow, H. B. PATTERN RECOGNITION AND THE RESPONSES OF SENSORY NEURONS. Annals of the New York Academy of Sciences 1969, 156, 872.
- (3) Marc, R. E.; Murry, R. F.; Basinger, S. F. Pattern Recognition of Amino Acid Signatures in Retinal Neurons. *J. Neurosci.* **1995**, *15* (7), 5106–5129.
- (4) Tanaka, K. Neuronal Mechanisms of Object Recognition. *Science* **1993**, 262 (5134), 685–688.
- (5) Behnia, R.; Clark, D. A.; Carter, A. G.; Clandinin, T. R.; Desplan, C. Processing Properties of ON and OFF Pathways for Drosophila Motion Detection. *Nature* **2014**, *512* (7515), 427–430.
- (6) Rosenblatt, F. The Perceptron: A Probabilistic Model for Information Storage and Organization in the Brain. *Psychol. Rev.* **1958**, *65*, 386–408.
- (7) Amari, S.-I. Learning Patterns and Pattern Sequences by Self-Organizing Nets of Threshold Elements. *IEEE Trans. Comput.* **1972**, C-21 (11), 1197–1206.
- (8) Hopfield, J. J. Neural Networks and Physical Systems with Emergent Collective Computational Abilities. *Proc. Natl. Acad. Sci. U. S. A.* 1982, 79 (8), 2554–2558.
- (9) Schmidhuber, J. Annotated History of Modern AI and Deep Learning. arXiv December 29, 2022. .

- (10) Holcomb, S. D.; Porter, W. K.; Ault, S. V.; Mao, G.; Wang, J. Overview on DeepMind and Its AlphaGo Zero AI. In *Proceedings of the 2018 International Conference on Big Data and Education*; ICBDE '18; Association for Computing Machinery: 2018; pp 67–71. DOI: 10.1145/3206157.3206174.
- (11) OpenAI. GPT-4 Technical Report. arXiv March 27, 2023. DOI: 10.48550/arXiv.2303.08774.
- (12) Radford, A.; Kim, J. W.; Hallacy, C.; Ramesh, A.; Goh, G.; Agarwal, S.; Sastry, G.; Askell, A.; Mishkin, P.; Clark, J.; Krueger, G.; Sutskever, I. Learning Transferable Visual Models From Natural Language Supervision. arXiv February 26, 2021.
- (13) Rombach, R.; Blattmann, A.; Lorenz, D.; Esser, P.; Ommer, B. High-Resolution Image Synthesis with Latent Diffusion Models. arXiv April 13, 2022. DOI: 10.48550/arXiv.2112.10752.
- (14) Kuzum, D.; Yu, S.; Wong, H.-S. P. Synaptic Electronics: Materials, Devices and Applications. *Nanotechnology* **2013**, *24* (38), 382001.
- (15) Zhang, F.; Li, C.; Li, Z.; Dong, L.; Zhao, J. Recent Progress in Three-Terminal Artificial Synapses Based on 2D Materials: From Mechanisms to Applications. *Microsyst. Nanoeng.* **2023**, *9* (1), 1–17.
- (16) Zhang, Q.; Yu, H.; Barbiero, M.; Wang, B.; Gu, M. Artificial Neural Networks Enabled by Nanophotonics. *Light Sci. Appl.* **2019**, 8 (1), 42.
- (17) Núñez, J.; Avedillo, M. J.; Jiménez, M.; Quintana, J. M.; Todri-Sanial, A.; Corti, E.; Karg, S.; Linares-Barranco, B. Oscillatory Neural Networks Using VO2 Based Phase Encoded Logic. *Front. Neurosci.* **2021**, *15*, 442.
- (18) Thomas, A. Memristor-Based Neural Networks. J. Phys. Appl. Phys. 2013, 46 (9), 093001.
- (19) Berco, D.; Shenp Ang, D. Recent Progress in Synaptic Devices Paving the Way toward an Artificial Cogni-Retina for Bionic and Machine Vision. *Adv. Intell. Syst.* **2019**, *1* (1), 1900003.
- (20) Corti, E.; Cornejo Jimenez, J. A.; Niang, K. M.; Robertson, J.; Moselund, K. E.; Gotsmann, B.; Ionescu, A. M.; Karg, S. Coupled VO2 Oscillators Circuit as Analog First Layer Filter in Convolutional Neural Networks. *Front. Neurosci.* **2021**, *15*, 19.
- (21) Carapezzi, S.; Delacour, C.; Plews, A.; Nejim, A.; Karg, S.; Todri-Sanial, A. Role of Ambient Temperature in Modulation of Behavior of Vanadium Dioxide Volatile Memristors and Oscillators for Neuromorphic Applications. *Sci. Rep.* **2022**, *12* (1), 19377.
- (22) Béteille, F.; Mazerolles, L.; Livage, J. Microstructure and Metal-Insulating Transition of Vo2 Thin Films. *Mater. Res. Bull.* **1999**, 34 (14), 2177–2184.
- (23) Cope, R. G.; Penn, A. W. High-Speed Solid-State Thermal Switches Based on Vanadium Dioxide. *J. Phys. Appl. Phys.* **1968**, *1* (2), 161.
- (24) Cao, J.; Ertekin, E.; Srinivasan, V.; Fan, W.; Huang, S.; Zheng, H.; Yim, J. W. L.; Khanal, D. R.; Ogletree, D. F.; Grossman, J. C.; Wu, J. Strain Engineering and One-Dimensional Organization of Metal-Insulator Domains in Single-Crystal Vanadium Dioxide Beams. *Nat. Nanotechnol.* **2009**, *4* (11), 732–737.
- (25) Wegkamp, D.; Stähler, J. Ultrafast Dynamics during the Photoinduced Phase Transition in VO2. *Prog. Surf. Sci.* **2015**, *90* (4), 464–502.
- (26) Lysenko, S.; Rua, A. J.; Vikhnin, V.; Jimenez, J.; Fernandez, F.; Liu, H. Light-Induced Ultrafast Phase Transitions in VO2 Thin Film. *Appl. Surf. Sci.* **2006**, 252 (15), 5512–5515.
- (27) Liu, W.-T.; Cao, J.; Fan, W.; Hao, Z.; Martin, M. C.; Shen, Y. R.; Wu, J.; Wang, F. Intrinsic Optical Properties of Vanadium Dioxide near the Insulator-Metal Transition. *Nano Lett.* **2011**, *11* (2), 466–470.
- (28) Perucchi, A.; Baldassarre, L.; Postorino, P.; Lupi, S. Optical Properties across the Insulator to Metal Transitions in Vanadium Oxide Compounds. *J. Phys.: Condens. Matter* **2009**, *21* (32), 323202.
- (29) Derkaoui, I.; Khenfouch, M.; Benkhali, M.; Rezzouk, A. VO2 Thin Films for Smart Windows: Numerical Study of the Optical Properties and Performance Improvement. *J. Phys. Conf. Ser.* **2019**, 1292 (1), 012010.

- (30) Radu, I. P.; Martens, K.; Govoreanu, B.; Mertens, S.; Shi, X.; Jurczak, M.; de Gendt, S.; Stesmans, A.; Kittl, J. A.; Heyns, M. Investigation of the Switching Behavior of Two-Terminal Devices on VO₂, 2011 Int. Conf. Solid State Dev. Mat., 2011, 138–139, https://doi.org/10.7567/SSDM.2011.P-4-6.
- (31) Liu, K.; Lee, S.; Yang, S.; Delaire, O.; Wu, J. Recent Progresses on Physics and Applications of Vanadium Dioxide. *Mater. Today* **2018**, *21* (8), 875–896.